where β is the divergence of the incident beam. While increasing the divergence angle β may introduce instrumental broadening which deteriorates the 2θ resolution, virtual oscillation improves sampling statistics without introducing instrumental broadening.

In the cases of materials with a large grain size or preferred orientation, or of microdiffraction with a small X-ray beam size, it can be difficult to determine the 2θ position because of poor counting statistics. In these cases, some kind of sample oscillation, either by translation or rotation, can bring more crystallites into the diffraction condition. Angular oscillation is an enhancement to the angular window of the instrument. The effect is that the angular window scans over the oscillation angle. Any of the three rotation angles (ω, ψ, φ) or their combinations can be used as oscillation angles. Angular oscillation can effectively improve the sampling statistics for both large grain size and preferred orientation. As an extreme example, a powder-diffraction pattern can be generated from single-crystal sample if a sufficient angular window can be achieved by sample rotation in such as way as to simulate a Gandolfi camera (Guggenheim, 2005). Sample oscillation is not always necessary if virtual oscillation can achieve sufficient sampling statistics.

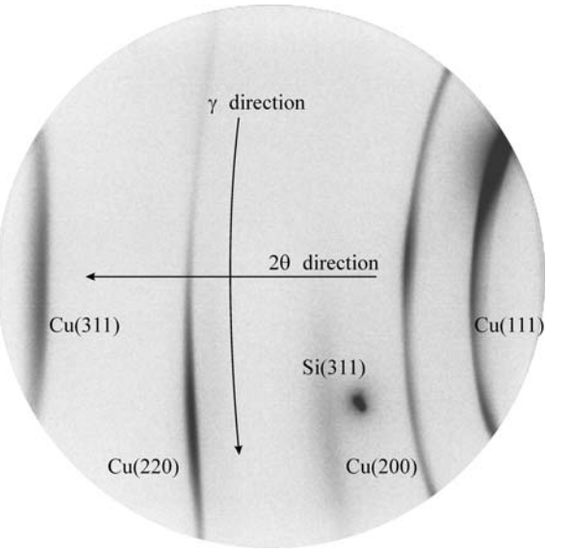

Figure 2.5.18
Diffraction frame collected from a Cu film on an Si substrate showing intensity variation along γ due to texture.

2.5.4.2. *Texture analysis*

Most natural or artificial solid materials are polycrystalline, consisting of many crystallites (also called grains) of various sizes, shapes and orientations. When the orientations of the crystallites in a material have a random distribution, it presents isotropic properties. The anisotropic orientation distribution of crystallites is referred to as preferred orientation or texture. Depending on the degree of the preferred orientation, a sample is referred to as having a weak, moderate or strong texture. Many electrical, optical or mechanical properties of materials are affected or determined by their texture. The determination and interpretation of textures are therefore of fundamental importance in materials science and technology (Bunge, 1983).

When a conventional X-ray diffractometer with a point detector is used for texture measurement, the crystallite orientation distribution in one direction is measured at a time, and full texture information is measured by rotating the sample to all the desired orientations. When a two-dimensional X-ray diffraction system is used for texture measurement, the orientation distributions of several crystallographic planes over a range of angles can be measured simultaneously so as to get better measurement results in a shorter data-collection time (Smith & Ortega, 1993; Blanton, 1994; Bunge & Klein, 1996; Helming *et al.*, 2003; Wenk & Grigull, 2003; He, 2009). The orientation relationships between different phases or between different layers of thin films and substrates can also be easily revealed. The texture effect may be observed and evaluated directly from the 2D diffraction frames without data processing.

2.5.4.2.1. *Pole density and pole figures*

XRD results from an 'ideal' powder in which the crystallites are randomly oriented normally serve as a basis for determining the relative intensity of each diffraction peak. The deviation of the grain orientation distribution of a polycrystalline material from that of an ideal powder is measured as texture. The pole figure for a particular crystallographic plane is normally used to represent the texture of a sample. Assuming that all grains have the same volume, each 'pole' represents a grain that satisfies the Bragg condition. The number of grains satisfying the Bragg condition at a particular sample orientation can be larger or smaller than the number of grains for an ideal sample, and likewise for the integrated intensity of that peak. The measured 2D diffraction pattern contains two very important parameters at each γ angle: the partially integrated intensity I and the Bragg angle 2θ. Fig. 2.5.18 shows a 2D frame for a Cu thin film on an Si wafer collected with a microgap 2D detector. It contains four Cu lines and one Si spot. The diffraction intensity varies along γ because of the anisotropic pole-density distribution. For each diffraction ring, the intensity is a function of γ and the sample orientation (ω, ψ, φ), *i.e.* $I = I(\gamma, \omega, \psi, \varphi)$.

Plotting the intensity of each (hkl) line with respect to the sample coordinates in a stereographic projection gives a qualitative view of the orientation of the crystallites with respect to a sample direction. These stereographic projection plots are called pole figures. As is shown in Fig. 2.5.19(a), the sample orientation is defined by the sample coordinates S_1, S_2 and S_3. For metals with rolling texture, the axes S_1, S_2 and S_3 correspond to the transverse direction (TD), rolling direction (RD) and normal direction (ND), respectively. Let us consider a sphere with unit radius and the origin at O. A unit vector representing an arbitrary pole direction starts from the origin O and ends at the point P on the sphere. The pole direction is defined by the radial angle α and azimuthal angle β. The pole density at the point P projects to the point P' on the equatorial plane through a straight line from P to the point S. The pole densities at all directions are mapped onto the equatorial plane by stereographic projection as shown in Fig. 2.5.19(b). This two-dimensional mapping of the pole density onto the equatorial plane is called a pole figure. The azimuthal angle β projects to the pole figure as a rotation angle about the centre of the pole figure from the sample direction S_1. When plotting the pole density into a pole figure of radius R, the location of the point P' in the pole figure should be given by β and

$$r = R\tan\left(\frac{\pi}{4} - \frac{\alpha}{2}\right) = R\tan\frac{\chi}{2}. \qquad (2.5.52)$$

For easy computer plotting and easy angular readout from the pole figure, the radial angle α may be plotted on an equally spaced angular scale, similar to a two-dimensional polar coordinate system. Other pole-figure mapping styles may be used, but must be properly noted to avoid confusion (Birkholz, 2006).

2.5.4.2.2. *Fundamental equations*

The α and β angles are functions of $\gamma, \omega, \psi, \varphi$ and 2θ. As shown in Fig. 2.5.19(*a*), a pole has three components h_1, h_2 and h_3, parallel to the three sample coordinates S_1, S_2 and S_3, respectively. The pole-figure angles (α, β) can be calculated from the unit-vector components by the following pole-mapping equations:

$$\alpha = \sin^{-1}|h_3| = \cos^{-1}(h_1^2 + h_2^2)^{1/2}, \tag{2.5.53}$$

$$\beta = \pm\cos^{-1}\frac{h_1}{(h_1^2 + h_2^2)^{1/2}} \qquad \begin{cases} \beta \geq 0^\circ \text{ if } h_2 \geq 0 \\ \beta < 0^\circ \text{ if } h_2 < 0 \end{cases}, \tag{2.5.54}$$

where α takes a value between 0 and 90° ($0^\circ \leq \alpha \leq 90^\circ$) and β takes values in two ranges ($0^\circ \leq \beta \leq 180^\circ$ when $h_2 > 0$ and $-180^\circ \leq \beta < 0^\circ$ when $h_2 < 0$). The condition for reflection-mode diffraction is $h_3 > 0$. For transmission diffraction it is possible that $h_3 < 0$. In this case, the pole with mirror symmetry about the S_1S_2 plane to the diffraction vector is used for the pole-figure mapping. The absolute value of h_3 is then used in the equation for the α angle. When $h_2 = 0$ in the above equation, β takes one of two values depending on the value of h_1 ($\beta = 0^\circ$ when $h_1 \geq 0$ and $\beta = 180^\circ$ when $h_1 < 0$). For Eulerian geometry, the unit-vector components $\{h_1, h_2, h_3\}$ are given by equation (2.5.11).

The 2θ integrated intensity along the diffraction ring is then converted to the pole-density distribution along a curve on the pole figure. The α and β angles at each point of this curve are calculated from ω, ψ, φ, γ and 2θ. The sample orientation (ω, ψ, φ) and 2θ for a particular diffraction ring are constants; only γ takes a range of values depending on the detector size and distance.

For a textured sample, the 2θ-integrated intensity of a diffraction ring from a family of (hkl) planes is a function of γ and the sample orientation (ω, ψ, φ), *i.e.* $I_{hkl} = I_{hkl}(\omega, \psi, \varphi, \gamma, \theta)$. From the pole-figure angle-mapping equations, we can obtain the integrated intensity in terms of pole-figure angles as

$$I_{hkl}(\alpha, \beta) = I_{hkl}(\omega, \psi, \varphi, \gamma, \theta). \tag{2.5.55}$$

The pole density at the pole-figure angles (α, β) is proportional to the integrated intensity at the same angles:

$$P_{hkl}(\alpha, \beta) = K_{hkl}(\alpha, \beta) I_{hkl}(\alpha, \beta), \tag{2.5.56}$$

where $I_{hkl}(\alpha, \beta)$ is the 2θ-integrated intensity of the (hkl) peak corresponding to the pole direction (α, β), $K_{hkl}(\alpha, \beta)$ is the scaling factor covering the absorption, polarization, background corrections and various instrument factors if these factors are included in the integrated intensities, and $P_{hkl}(\alpha, \beta)$ is the pole-density distribution function. Background correction can be done during the 2θ integration and will be discussed in Section 2.5.4.2.4. The pole figure is obtained by plotting the pole-density function based on the stereographic projection.

The pole-density function can be normalized such that it represents a fraction of the total diffracted intensity integrated over the pole sphere. The normalized pole-density distribution function is given by

$$g_{hkl}(\alpha, \beta) = \frac{2\pi P_{hkl}(\alpha, \beta)}{\int_0^{2\pi}\int_0^{\pi/2} P_{hkl}(\alpha, \beta)\cos\alpha \, \mathrm{d}\alpha \, \mathrm{d}\beta}. \tag{2.5.57}$$

The pole-density distribution function is a constant for a sample with a random orientation distribution. Assuming that the sample and instrument conditions are the same except for the pole-density distribution, we can obtain the normalized pole-density function by

$$g_{hkl}(\alpha, \beta) = \frac{I_{hkl}(\alpha, \beta)}{I_{hkl}^{\text{random}}(\alpha, \beta)}. \tag{2.5.58}$$

The integrated intensity from the textured sample without any correction can be plotted according to the stereographic projection as an 'uncorrected' pole figure. The same can be done for the sample with a random orientation distribution to form a 'correction' pole figure that contains only the factors to be corrected. The normalized pole figure is then obtained by dividing the 'uncorrected' pole figure by the 'correction' pole figure. This experimental approach is feasible only if a similar sample with a random orientation distribution is available.

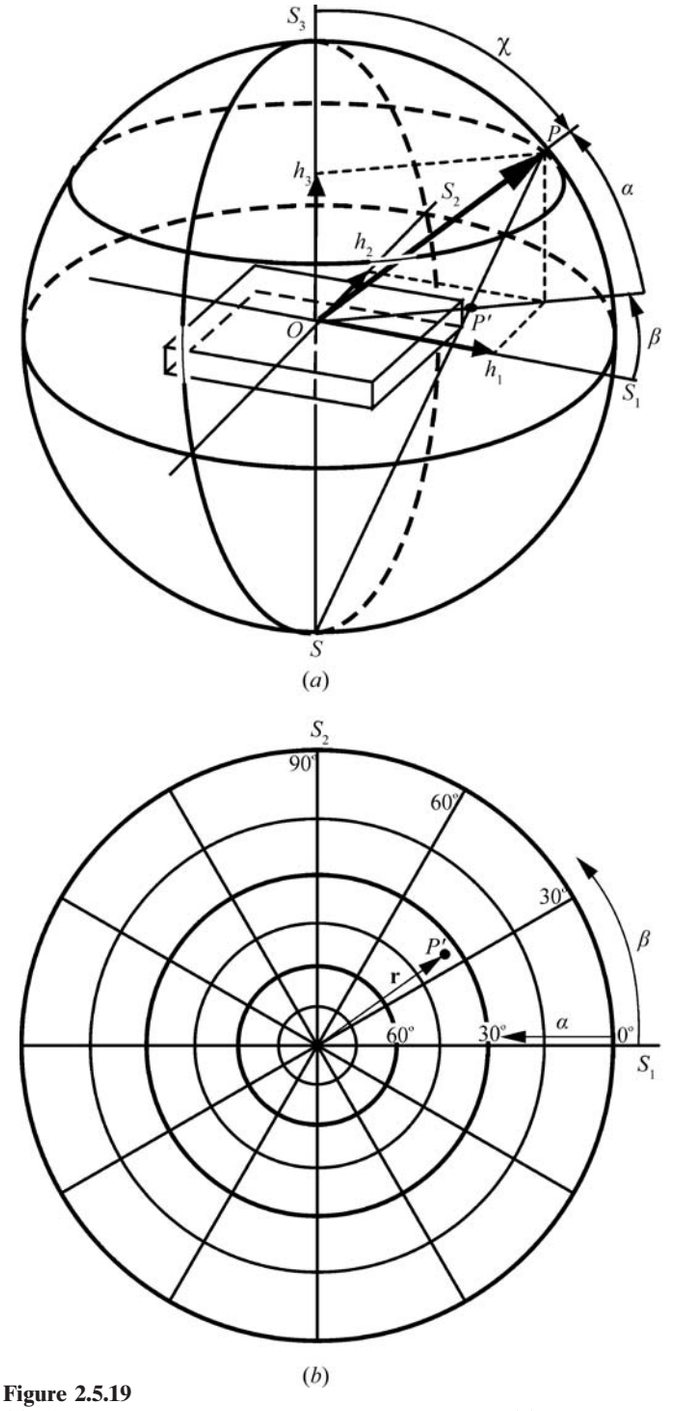

Figure 2.5.19
(*a*) Definition of pole direction angles α and β; (*b*) stereographic projection in a pole figure.

If the texture has a rotational symmetry with respect to an axis of the sample, the texture is referred to as a fibre texture and the axis is referred to as the fibre axis. The sample orientation containing the symmetry axis is referred to as the fibre axis. The fibre texture is mostly observed in two types of materials: metal wires or rods formed by drawing or extrusion, and thin films formed by physical or chemical deposition. The fibre axis is the wire axis for a wire and normal to the sample surface for thin films. Fibre texture can also be artificially formed by rotating a sample about its normal. If the fibre axis is aligned to the S_3 direction, the pole-density distribution function becomes independent of the azimuthal angle β. For samples with fibre texture, or artificially formed fibre texture by rotating, the pole-density function is conveniently expressed as a function of a single variable, $g_{hkl}(\chi)$. Here, χ is the angle between the sample normal and pole direction.

$$\chi = 90^\circ - \alpha \text{ or } \chi = \cos^{-1}|h_3|. \qquad (2.5.59)$$

The pole-density function for fibre texture can be expressed as a fibre plot. The fibre plot $g_{hkl}(\chi)$ can be calculated from the relative intensity of several peaks (He, 1992; He *et al.*, 1994) and artificial fibre texture can be achieved by sample spinning during data collection.

2.5.4.2.3. *Data-collection strategy*

Since a one-dimensional pole-density mapping is created from each 2D frame, it is important to lay out a data-collection strategy so as to have the optimum pole-figure coverage and minimum redundancy in data collection. The pole-figure coverage can be simulated from the diffraction 2θ angle, detector swing angle, detector distance, goniometer angles and scanning steps. When a large 2D detector is placed close to the sample, it is possible to collect a pole figure with a single φ scan. Fig. 2.5.20(a) shows an example of a scheme generated by a single φ scan of 5° steps with a detector 10.5 cm in diameter and D = 7 cm. The data collected with a single exposure at $\varphi = 0^\circ$ would generate a one-dimensional pole figure as shown in the curve marked by A and B. The pole figure can be generated by a full-circle rotation of 360°. The pole density at the centre represents the diffraction vector perpendicular to the sample surface. It is important to have the pole-density information in the centre region of the pole figure, especially for fibre texture. The pole-figure angle at the centre is $\alpha = 90^\circ$, and the best strategy is to put point A at the centre of pole figure. That is

$$h_3^A = \sin\theta\cos\psi\sin\omega - \cos\theta\sin\gamma_A\cos\psi\cos\omega - \cos\theta\cos\gamma_A\sin\psi = 1. \qquad (2.5.60)$$

In some cases, a single φ scan is not enough to cover sufficient pole-figure angles because of a large detector distance or limited detector area, so it is necessary to collect a set of data with φ scans at several different sample tilt angles. Fig. 2.5.20(b) illustrates the data-collection scheme with a detector that is 10.5 cm in diameter and D = 10 cm for the (111) plane of a Cu thin film. In this case, each pole figure requires two φ scans at different sample orientations. The data-collection strategy should also be optimized for several crystallographic planes if all can be covered in a frame. The step size of the data-collection scan depends highly on the strength of the texture and the purpose of the texture measurements. For a weak texture, or quality control for metal parts, φ (or ω, or ψ) scan steps of 5° may be sufficient. For strong textures, such as thin films with epitaxial structure, scan steps of 1° or smaller may be necessary.

The effectiveness of two-dimensional data collection for a texture can be compared with that using a point detector with the data-collection strategy of the Cu thin film as an example. Fig. 2.5.20(c) shows the pole-figure data-collection strategy with a point detector. For the same pole-figure resolution, significantly more exposures are required with a point detector. Considering that several diffraction rings are measured simultaneously with a 2D detector, the pole-figure measurement is typically 10 to 100 times faster than with a point detector. Therefore, quantitative high-resolution pole-figure measurements are only practical with a 2D-XRD system (Bunge & Klein, 1996).

2.5.4.2.4. *Texture-data processing*

For a specific diffraction ring, 2θ is a constant or at least assumed to be constant for texture analysis, and the sample-orientation angles (ω, ψ, φ) for a frame are also constants. Therefore, the pole-density information is given by the diffraction-intensity distribution as a function of γ only, or $I = I(\gamma)$. Integration of the diffraction intensities in the 2θ direction converts 2D information into the function $I(\gamma)$.

Fig. 2.5.21(a) shows a 2D diffraction ring for texture analysis. The low and high background and diffraction-ring 2θ–γ range are defined by three boxes, noted as B_L, B_H and $I(\gamma)$, respectively. All three boxes have the same γ range from γ_1 to γ_2. The 2θ ranges for the diffraction ring, low background and high background should be determined based on the width of the 2θ peak and available background between adjacent peaks. Assuming a normal distribution, a 2θ range of 2 times the FWHM covers 98% of the intensity peak, and 3 times the FWHM covers more than 99.9%. The 2θ range should also be broad enough to cover the possible 2θ shifts caused by residual stresses in the sample. Fig. 2.5.21(b) is the 2θ profile integrated over the section $\Delta\gamma$ in Fig. 2.5.21(a). The background ranges on the low and high 2θ sides are given by $2\theta_{L1}$–$2\theta_{L2}$ and $2\theta_{H1}$–$2\theta_{H2}$, respectively. The 2θ-integrated diffraction intensities as a function of γ are plotted in Fig. 2.5.21(c). The background can be calculated and removed from the intensity values of the low and high backgrounds or ignored if the contribution of the background is very small.

2θ integration without a background correction can be

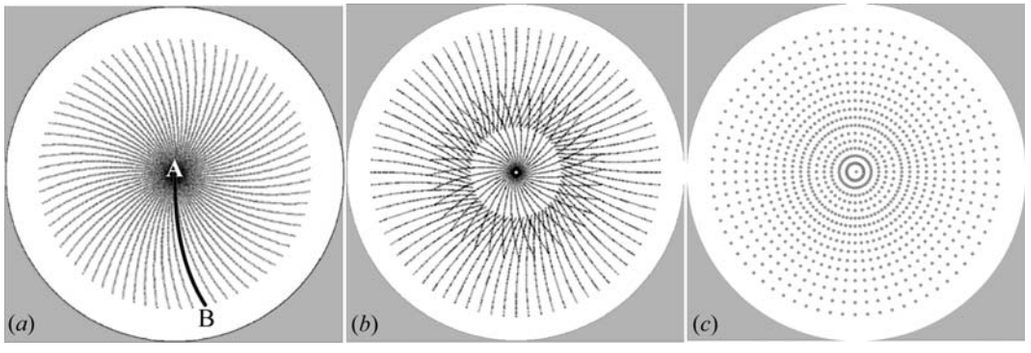

Figure 2.5.20
Data-collection strategy: (a) 2D detector with D = 7 cm; (b) 2D detector with D = 10 cm; (c) point detector.

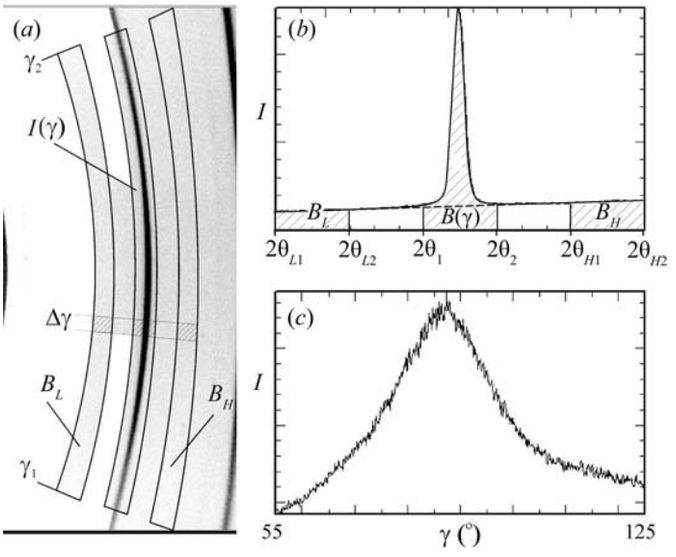

Figure 2.5.21
Pole-figure data processing: (*a*) a frame with the 2θ integration ranges for the (220) ring; (*b*) 2θ profile showing the background and peak; (*c*) integrated intensity distribution as a function of γ.

expressed as

$$I(\gamma) = \int_{2\theta_1}^{2\theta_2} J(2\theta, \gamma)\, \mathrm{d}(2\theta), \quad \gamma_1 \le \gamma \le \gamma_2. \tag{2.5.61}$$

A similar equation can be used for 2θ integration of the low and high backgrounds $B_L(\gamma)$ and $B_H(\gamma)$. Assuming a linear background change in the vicinity of the 2θ peak, the background under the peak, $B(\gamma)$, is then given by

$$B(\gamma) = B_L(\gamma)\frac{(2\theta_2 - 2\theta_1)(2\theta_{H2} + 2\theta_{H1} - 2\theta_2 - 2\theta_1)}{(2\theta_{L2} - 2\theta_{L1})(2\theta_{H2} + 2\theta_{H1} - 2\theta_{L2} - 2\theta_{L1})} + B_H(\gamma)\frac{(2\theta_2 - 2\theta_1)(2\theta_2 + 2\theta_1 - 2\theta_{L2} - 2\theta_{L1})}{(2\theta_{H2} - 2\theta_{H1})(2\theta_{H2} + 2\theta_{H1} - 2\theta_{L2} - 2\theta_{L1})}. \tag{2.5.62}$$

Then the background $B(\gamma)$ can be subtracted from the integrated intensity distribution $I(\gamma)$.

The algorithms of γ integration given in Section 2.5.4.2.3 can be easily modified for 2θ integration by exchanging γ and 2θ in the equations. Algorithms with solid-angle normalization should be used to get consistent integrated intensity over all areas of the detector. The 2θ-integrated intensity distribution can then be mapped onto a pole figure based on the fundamental equations (2.5.53) and (2.5.54). When a pole-figure pixel is overlapped by more than one data point from different scans, as shown in the region covered by two scans in Fig. 2.5.20(*b*), the average value should be mapped to that pole-figure pixel. Fig. 2.5.22(*a*) shows pole-density mappings on the pole figure. There are big gaps between the measured pole-density data points due to the large φ-scan steps of 5°.

All factors affecting relative intensities, such as Lorentz, polarization, air scattering, and Be-window and sample absorption, will have an effect on the measured pole densities for the pole figures. Some or all these corrections may be applied to the diffraction frames before 2θ integration if the texture study demands high accuracy in the relative pole densities. Among these factors, the most important factor is sample absorption, since data sets for pole figures are typically collected at several different incident angles. A ridge between the pole-density regions covered by two different incident angles may be observed if sample absorption is not properly corrected.

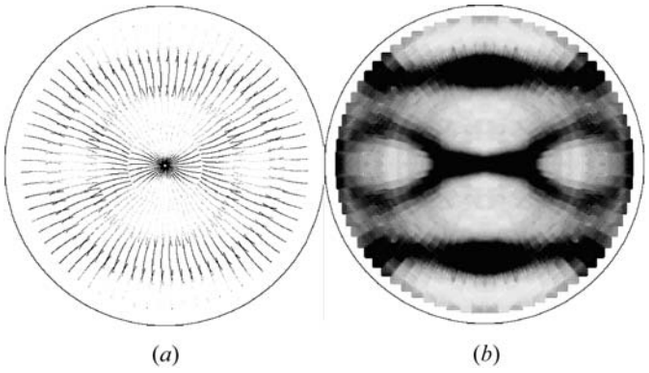

Figure 2.5.22
Pole-figure processing: (*a*) $I(\gamma)$ mapped to the pole figure; (*b*) Pole figure after interpolation and symmetry processing.

2.5.4.2.5. *Pole-figure interpolation and use of symmetry*

The pole figure is stored and displayed as a bitmap image. The pole-density data from the data set may not fill up all the pixels of the pole-figure image. In order to generate a smooth pole figure, the unmapped pixels are filled with values generated from the interpolation of the surrounding pixels. A linear interpolation within a defined box is sufficient to fill the unmapped pixels. The size of the box should be properly chosen. A box that is too small may not be able to fill all unmapped pixels and a box that is too big may have a smearing effect on the pole figure, especially if a sharp pole figure is processed. All the gaps between the measured pole-density points are filled after this interpolation. For a sample with sharp texture, smaller φ-scan steps should be used.

All pole figures possess symmetry as a consequence of the Laue symmetry of the crystallites in the sample. This symmetry can be used to fill in values for pixels in the pole figure for which data were not measured, or to smooth the pole figure. For example, orthorhombic materials exhibit *mmm* symmetry, thus one needs to collect only an octant or quadrant of the pole sphere to generate the entire pole figure. The pole figures of materials with higher symmetry may be treated by using lower symmetry in the processing. For instance, one can use 2/*m* or *mmm* symmetry for hexagonal materials and *mmm* for cubic materials. In symmetry processing, all the symmetry-equivalent pole-figure pixels are filled by the average value of the measured pixels. For the unmeasured pole-figure pixels, this symmetry processing fills in a value from the average of all the equivalent pixels. For the measured pixels, this average processing serves as a smoothing function. Fig. 2.5.22(*b*) shows the results after both interpolation and use of symmetry.

2.5.4.2.6. *Orientation relationship*

A 2D-XRD system can measure texture from a sample containing a single phase, multiple phases or single crystals. The orientation relationship between different phases, or thin films and substrates, can be revealed because data are collected from all phases of the sample simultaneously. One example is the measurement of pole figures for a magnetron sputter-deposited Cu film on an Si wafer (He *et al.*, 2005). Fig. 2.5.23 shows the overlapped pole figures of the Cu (111) film and Si (400) substrate in a 2D pole figure (*a*) and 3D surface plot (*b*). The three sharp spots from the (400) spots of the Si wafer show the wafer cut orientation of (111). The Cu (111) pole density maxi-

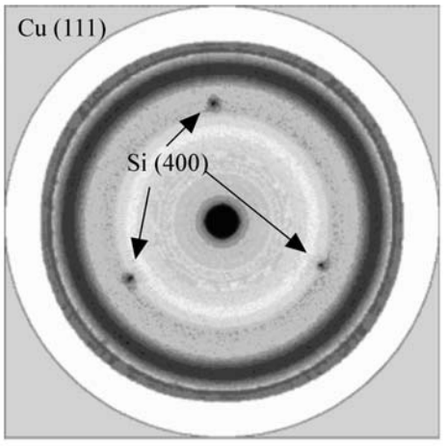

(*a*)

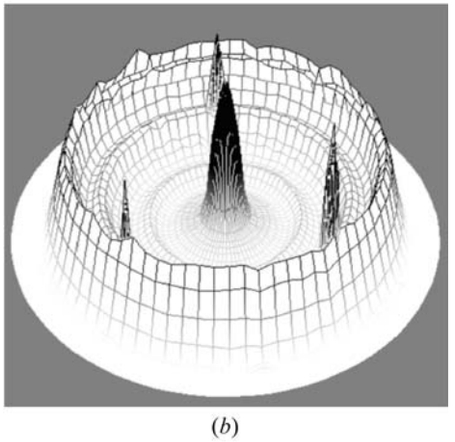

(*b*)

Figure 2.5.23
Combined pole figure of a Cu (111) film on an Si (400) substrate: (*a*) regular 2D projection; (*b*) 3D surface plot.

mized in the centre of the pole figure shows a strong (111) fibre texture. The orientation relationship between the film fibre axis and the substrate is clearly described by the combined pole figures. For samples containing multiple thin-film layers, the orientation relationships between the different layers of the films and substrate can be revealed by superimposing their pole figures.

2.5.4.3. *Stress measurement*

When a solid material is elastically deformed by a force, each crystallite in it changes shape or size. Assuming that the stresses in each crystallite represent the stresses in the solid, the stresses can be measured by measuring the lattice *d*-spacing changes in the crystallites. These *d*-spacing changes can be measured by the changes in diffraction-peak positions based on Bragg's law. In this case, the *d*-spacing serves as a gauge of the deformation. Stress measurement by X-ray diffraction is typically done using a point detector or line detector (Walter, 1971; James & Cohen, 1980; Noyan & Cohen, 1987; Lu, 1996); this will be referred to as the conventional method. The stress or stress tensor is calculated from many strain measurements from diffraction-peak 2θ shifts of a specific lattice-plane family. With a point or line detector, only a small cross section of the diffraction cone is measured at one sample orientation (ψ, φ). Compared to using a conventional detector, 2D detectors have many advantages in stress measurement (Borgonovi, 1984; Korhonen *et al.*, 1989; Yoshioka & Ohya, 1992; Fujii & Kozaki, 1993; He & Smith, 1997; Kämpfe *et al.*, 1999; Hanan *et al.*, 2004). Since a 2D diffraction pattern covers the whole or a large portion of the diffraction rings, it can be used to measure stress with higher accuracy and can be collected in a shorter time than a conventional diffraction pattern, especially when dealing with highly textured materials, large grain sizes, small sample areas, weak diffraction, stress mapping and stress-tensor measurement. The 2D method for stress measurement is based on the fundamental relationship between the stress tensor and the diffraction-cone distortion (He & Smith, 1997; He, 2000; European Standard, 2008).

There are two kinds of stresses, which depend on the source of the loading forces that produce them. One kind is applied stress, caused by external forces acting on the solid object. Applied stress changes when the loading forces change and it disappears once the forces are removed. The stresses measured by X-ray diffraction method are mostly residual stresses. Residual stress is caused by internal forces between different parts of a solid body. Residual stress exists without external forces or remains after the external forces have been removed. The net force and moment on a solid body in equilibrium must be zero, so the residual stresses in the body must be balanced within the body. This means that a compressive stress in one part of the body must come with a tensile stress in another part of the body. For example, the residual stress in a thin film is balanced by the stresses in the substrate. When residual stress in a solid body is mentioned it typically refers to a specific location.

Residual stresses are generally categorized as macroscopic or microscopic depending on the range over which the stresses are balanced. The macroscopic residual stress is the stress measured over a large number of grains. This kind of stress can be measured by X-ray diffraction through the shift of the Bragg peaks. The microscopic stress is the stress measured over one or a few grains, or as small a range as micro- or nanometres. This kind of stress alone will not cause a detectable shift of diffraction peaks, but is reflected in the peak profiles. In this chapter, we will focus on the X-ray diffraction method for stress measurement at the macroscopic level.

2.5.4.3.1. *Stress and strain relation*

Stress is a measure of the deforming force applied to a solid per unit area. The stress on an elemental volume in the sample coordinates S_1, S_2, S_3 contains nine components, given by

$$\sigma_{ij} = \begin{bmatrix} \sigma_{11} & \sigma_{12} & \sigma_{13} \\ \sigma_{21} & \sigma_{22} & \sigma_{23} \\ \sigma_{31} & \sigma_{32} & \sigma_{33} \end{bmatrix}. \tag{2.5.63}$$

A component is normal stress when the two indices are identical, or shear stress when the two indices differ. The group of the nine stress components is called the stress tensor. The stress tensor is a tensor of the second order. Under equilibrium conditions, the shear components must maintain the following relations:

$$\sigma_{12} = \sigma_{21},\ \ \sigma_{23} = \sigma_{32} \text{ and } \sigma_{31} = \sigma_{13}. \tag{2.5.64}$$

Therefore, only six independent components define the stress state in a solid. The following stress states are typically measured:

Uniaxial: all stress components are zero except one normal stress component.

Biaxial: all nonzero components are within the S_1S_2 plane.

Biaxial with shear: $\sigma_{33} = 0$, all other components are not necessarily zero.

Equibiaxial: a special case of biaxial stress where $\sigma_{11} = \sigma_{22} = \sigma$.